

# INTERPRETING THE BEHAVIOR OF TIME-RESOLVED GAMMA-RAY BURST SPECTRA

NICOLE M. LLOYD-RONNING<sup>1</sup> AND VAHÉ PETROSIAN<sup>2</sup>

Center for Space Science and Astrophysics, Stanford University, Stanford, CA 94305; nicole@urania.stanford.edu

Received 2001 June 6; accepted 2001 September 19

## ABSTRACT

In this paper, we explore time-resolved gamma-ray burst (GRB) spectra in the context of the synchrotron emission model presented by Lloyd & Petrosian in 2000. First, we show that our model—which involves three distinct emission regimes—can provide excellent fits to the time-resolved spectra of GRBs, and we present these results for a few bursts. We then describe how the phenomenological Band spectrum can be interpreted in the context of our models based on the value of the low-energy photon index  $\alpha$ . We discuss the types of correlations one would expect to observe among the Band parameters if these models are correct. We then compare these predictions to the existing data, combining a sample of 2026 time-resolved spectra (from approximately 80 bursts). We show that the correlations found in the data are consistent with the models and discuss the constraints they place on the emission physics. In particular, we find a ( $\sim 4\sigma$ ) negative correlation between the peak of the  $\nu F_\nu$  spectrum  $E_p$  and the low-energy photon index  $\alpha$  for bursts with  $-\frac{2}{3} < \alpha < 0$ , in contrast to what is predicted by the instrumental effect discussed in Lloyd & Petrosian. We suggest that this correlation is simply due to the mechanism responsible for producing values of  $\alpha$  above the value of  $-\frac{2}{3}$ —namely, a decreasing mean pitch angle of the electrons. We also show that  $E_p$  is correlated with the photon flux and interpret this as a result of changing magnetic field or characteristic electron energy between emission episodes. Finally, we discuss the implications that our results have on particle acceleration in GRBs and prospects for further testing these models with the anticipated data from the *High Energy Transient Explorer 2*, *Swift*, and the *Gamma-Ray Large Area Space Telescope*.

*Subject headings:* gamma rays: bursts — radiation mechanisms: nonthermal

## 1. INTRODUCTION

Except for a few isolated bursts (see, e.g., Tavani 1996; Brainerd et al. 1996), most of the analyses of the *prompt* spectral data of gamma-ray bursts (GRBs) have employed phenomenological models—in most cases, using the so-called Band spectrum (Band et al. 1993). This model is essentially a smoothly broken power law with a low-energy photon spectral index  $\alpha$ , a high-energy photon index  $\beta$ , and a break energy  $E_p$ . It has been shown that such a model describes most GRB spectra very well (see, e.g., Mallozzi et al. 1996; Lloyd & Petrosian 1999; Preece et al. 2000). There have been some attempts to explain or interpret some of the global properties of these spectral parameters in terms of a physical model (see, e.g., Totani 1999; Preece et al. 1998b; Ghisellini, Celotti, & Lozzati 2000) with inconclusive results. In Lloyd & Petrosian (2000, hereafter LP00), we showed that realistic synchrotron models can qualitatively explain the global distributions of the time-averaged Band spectral parameters. Our model modified the usual simple picture of optically thin synchrotron emission from a power-law distribution of electrons with a sharp low-energy cutoff by accounting for (1) the possibility of a smooth cutoff to the low-energy electron distribution, (2) radiation from an anisotropic electron distribution with a small mean pitch angle, (3) synchrotron self-absorption, and (4) the important instrumental effect in which the value of the fitted parameter  $\alpha$  decreases as  $E_p$  approaches the lower edge of the BATSE window. We have envisioned a realistic scenario in which particle acceleration and synchrotron losses

occur continually and simultaneously behind an internal shock (which produces a single pulse in the GRB time profile) with the characteristic acceleration time shorter than the loss time so that synchrotron loss effects are only evident in the particle distribution spectrum at energies much larger than what is relevant for our discussion here (at energies where the inequality is reversed and the loss time becomes shorter than the acceleration time). This model stands up well to the global distributions of GRB parameters. In particular, it can accommodate the bursts with  $\alpha$  above the so-called line-of-death value  $\alpha = -\frac{2}{3}$  (Preece et al. 1998b). However, the tests conducted so far have involved time-averaged properties of the bursts. Since each pulse is regarded as a separate emission episode (or internal shock) in our model, the averaging over many pulses may obscure the real physics of each episode. It would, therefore, be useful to examine the *time-resolved* spectral properties of GRBs so that one may compare the values and the *correlations* between the spectral parameters from pulse to pulse and perhaps within a pulse in hopes of gaining insight into the evolution of physical parameters throughout a GRB.

The temporal evolution of GRB spectral parameters has been studied by several authors (e.g., Norris et al. 1986; Kargatis et al. 1994; Ford et al. 1995; Crider et al. 1997; Preece et al. 1998b; Ryde & Svensson 2000). These studies have attempted to look for global trends in the data—in particular, Norris et al. and Ford et al. report a hard-to-soft evolution trend, while Crider et al. report both a hard-to-soft and a “tracking” trend (in which one or more spectral parameters track the time profile of the burst). The temporal behavior has not been rigorously interpreted in terms of an emission scenario (although Crider et al. attempt to explain at least the hard-to-soft evolution as evidence of a Comptonized spectrum in which the medium is expanding, causing  $E_p$  to decrease with time). Furthermore, with the

<sup>1</sup> Present address: Canadian Institute for Theoretical Astrophysics, University of Toronto, 60 St. George Street, Toronto ON M5S 3H8, Canada.

<sup>2</sup> Other affiliation: Departments of Physics and Applied Physics, Stanford University, Stanford, CA 94305.

exception of Kargatis et al., these studies have perhaps oversimplified the extremely varied and complex evolutionary behavior seen in most GRBs.

The purpose of this paper is to use our synchrotron emission models as diagnostics for interpreting the time-resolved GRB spectral parameters. Using a physical model—rather than a phenomenological model such as the Band spectrum—to characterize the GRB spectra allows us to gain insight into the evolution of actual physical parameters in the GRB plasmas. For example, in the case of optically thin emission by an isotropic distribution of electrons  $E_p \propto \gamma_m^2 B_\perp$ , where  $\gamma_m$  is the characteristic cutoff or turnover energy of the electron distribution and  $B_\perp$  is the perpendicular component of the magnetic field, the evolution of  $E_p$  reflects the evolution of  $\gamma_m$  and/or  $B_\perp$ . Clearly, just examining the evolution of this one spectral parameter will not lead to insights on the evolution of a single physical quantity since the former ( $E_p$ ) depends on more than one physical variable ( $\gamma_m$ ,  $B_\perp$ ). However, examining the evolution of this parameter and its *correlation* with other spectral parameters can help break some of the degeneracies, and the temporal behavior of the plasma parameters can begin to be elucidated.

Furthermore, once we get a handle on these parameters and their evolution throughout the GRB event, we can begin to gain some insight into the fundamental problem of particle acceleration in GRBs. The particle acceleration and loss (e.g., to radiation and otherwise) mechanisms determine the emitting electron distribution. The physics behind the particle acceleration determines the value of the minimum and maximum electron Lorentz factors, the smoothness of the low-energy cutoff to the electron distribution, the high-energy power-law index  $p$  of the electron distribution, and is of course intimately related to the magnetic field. The presence of a significant number of bursts with steep high-energy spectra—that is, with a high-energy photon index  $\beta = -(p+1)/2$  less than about  $-3$ —suggests that  $p$  can be significantly larger than the so-called universal index  $p \approx 2.2$  due to first-order Fermi acceleration in a relativistic shock (see, e.g., Kirk et al. 2000 and references therein); thus, a different type of particle acceleration mechanism may be at work. Furthermore, the evidence for the presence of synchrotron radiation from electrons with small pitch angles (see LP00 and below) also suggests that the usual assumption of isotropic distribution of the particle spectrum on short timescales may not be warranted. It is clear then that a burst's spectrum can help guide us in a detailed study of particle acceleration in internal shocks.

In this paper we will further develop and explain our synchrotron emission models and then use them to examine the behavior of the time-resolved GRB spectra in the context of an internal shock scenario. In § 2, we review the characteristics of our synchrotron models and show that these models provide good fits to the existing data. In § 3, we discuss the types of correlations expected among the spectral parameters in the context of our models.

In § 4, we examine correlations present between spectral parameters from Band fits carried out by Preece et al. (2000) in a sample of 2026 time-resolved spectra.

We find a strong positive correlation between the total photon flux  $f_\gamma$  and the peak of the  $\nu F_\nu$  spectrum  $E_p$  and correlations between  $E_p$  and the low-energy photon index  $\alpha$ , which differ depending on whether  $\alpha$  is above or below the value of roughly  $-\frac{2}{3}$ .

We interpret these results in the context of our models as reflecting changes in the physical parameters from one emission episode to the next (one internal shock to the next). In § 5, we present a few cases of spectral evolution for individual bursts simply to illustrate how the models can be used to infer something about the physics in a particular burst (from shock episode to shock episode).

Finally, in § 6, we present conclusions and discuss the implications of our results on particle acceleration in GRBs.

## 2. SOME DISTINCT SYNCHROTRON EMISSION SCENARIOS

The details of our synchrotron emission models are described in LP00, where it is shown that the low-energy spectral index  $\alpha$  plays a key role in understanding the emission mechanism(s) at hand. In this section, we describe three possible emission scenarios with distinct asymptotic low-energy spectral behavior.

### 2.1. Isotropic Pitch-Angle Distribution (IPD) of Electrons

This is the familiar optically thin synchrotron emission from a power-law electron energy spectrum, with an isotropic pitch-angle distribution, but, in contrast to most analyses, here we consider an electron distribution with a smooth low-energy cutoff:  $N(\gamma) \propto \{(\gamma/\gamma_m)^q/[1 + (\gamma/\gamma_m)^{p+q}]\}$ . Note that for high energies ( $\gamma > \gamma_m$ ), the spectrum goes as  $\gamma^{-p}$ , while for low energies ( $\gamma < \gamma_m$ ), the spectrum goes as  $\gamma^q$ . Hence,  $q$  denotes the steepness of the electron low-energy cutoff [note that an actual “cutoff,” in the sense that  $N(\gamma) \rightarrow 0$  as  $\gamma \rightarrow 0$ , requires  $q > 0$ ]. The asymptotic behavior of the synchrotron (photon number) spectrum for  $q > -\frac{1}{3}$  is

$$F_\gamma = \begin{cases} \nu^{-2/3}, & \nu \ll \nu_m = \frac{2}{3}\nu_B \sin^2 \Psi \gamma_m^2, \\ \nu^{-(p+1)/2}, & \nu \gg \nu_m, \end{cases} \quad (1)$$

where  $F_\gamma$  is the photon flux,  $\Psi$  is the electron pitch angle, and  $\nu_B = eB/m_e c$ , where  $B$  is the magnetic field. Note that the peak of the  $\nu F_\nu$  spectrum will occur at  $E_p \propto \nu_m \propto B \sin^2 \Psi \gamma_m^2$  and that the asymptotic low-energy index below this break is  $\alpha = -\frac{2}{3}$ . We point out that if  $q < -\frac{1}{3}$ , the low-energy asymptotic index is  $\alpha = (q-1)/2$ ; since  $q < -\frac{1}{3}$  does not constitute a cutoff, we do not discuss this further and limit our discussion to cases with  $0 < q < \infty$ . However, even though the low-energy asymptotic index of the photon spectrum is always  $-\frac{2}{3}$  for these (latter) cases, this does not mean that the value of  $q$  does not play an important role in the observed spectrum. As shown in LP00 and discussed in § 3, the smaller the value of  $q$  is, the lower the frequency at which the asymptotic value of  $-\frac{2}{3}$  is reached; because of the finite width of the detector spectral window, this can cause the fitted value of  $\alpha$  to be significantly less than  $-\frac{2}{3}$ .

### 2.2. Small Pitch-Angle Distribution (SPD) of Electrons

This spectrum results from optically thin synchrotron emission by electrons with a mean pitch angle  $\Psi \ll 1$ ; the analysis of synchrotron radiation in this regime was first done by Epstein (1973). For high-density, low magnetic field plasmas, the Alfvén phase velocity is less than the speed of light and (therefore) the speed of the relativistic particles under consideration here. In this case, the pitch-angle diffusion rate of the electrons interacting with plasma turbulence is much larger than the acceleration rate; consequently, the accelerated electrons will have an isotropic pitch-angle distribution. However, for the *low-density, high magnetic field*

conditions expected for the sources of GRBs, the opposite is true. In this case, the amplitude of the electric field fluctuations exceeds that of the magnetic field so that the above situation is reversed (see, e.g., Dung & Petrosian 1994; Pryadko & Petrosian 1998). Then the pitch-angle distribution of the accelerated electrons could become highly anisotropic as required in the small pitch-angle model. The shape of this spectrum depends on just how small the pitch angle is. For  $\Psi \ll 1$  but  $\Psi\gamma_m \sim 1$ , we have

$$F_\gamma = \begin{cases} \nu^0, & \nu \ll \nu_s = \frac{2}{3}\nu_B/(\gamma_m \Psi^2), \\ \nu^{-2/3}, & \nu_s \ll \nu \ll \nu_m, \\ \nu^{-(p+1)/2}, & \nu_m \gg \nu. \end{cases} \quad (2)$$

There are two breaks in this spectrum—one at  $\nu_m$  and one at  $\nu_s$ . Because the Band spectrum can only accommodate one break, spectral fits to this model will put the parameter  $E_p$  at one or the other of these two breaks but most likely at  $\nu_m$  because for  $p > 5/3$  (or for high-energy photon index  $\beta < -4/3$ , which is the case for most bursts), the break across  $\nu_m$  is more pronounced than across  $\nu_s$ . In this case, the low-energy photon index  $\alpha$  will fall somewhere between  $-2/3$  and 0.

However, as the pitch angle  $\Psi$  decreases such that  $\Psi \ll 1/\gamma_m$ , then the  $\nu^{-2/3}$  portion of the spectrum disappears, and only the  $\nu^0$  portion is left. In this case, we have

$$F_\gamma = \begin{cases} \nu^0, & \nu \ll \nu_s = \frac{4}{3}\nu_B \gamma_m, \\ \nu^{-(p+1)/2}, & \nu_s \gg \nu, \end{cases} \quad (3)$$

where  $E_p \propto B\gamma_m$  (see Epstein 1973 for a more detailed description of the behavior of the spectrum in this regime). We note that Medvedev 2000 has developed a model in which the transverse deflections of electrons in highly non-uniform, small-scale magnetic fields are smaller than the electrons' relativistic beaming angles [ $\sim 1/\gamma_e$ ], so that the entire trajectory of the electron is observable. In this case, a so-called jitter spectrum is obtained [Medvedev 2000] that has some of the same low-energy characteristics as the SPD spectrum—in particular, the low-energy photon index in this model also has a value of 0.)

### 2.3. Self-absorbed Spectrum (SAS)

If the magnetic field and density are such that the medium becomes optically thick to the synchrotron photons with frequency  $\nu < \nu_a$ , then for  $\nu_a < \nu_m$ , we have the following spectrum:

$$F_\gamma = \begin{cases} \nu^1, & \nu \ll \nu_a, \\ \nu^{-2/3}, & \nu_a \ll \nu \ll \nu_m, \\ \nu^{-(p+1)/2}, & \nu_m \gg \nu. \end{cases} \quad (4)$$

In that case,  $E_p \propto \nu_a \sim 10(nl)^{3/5} B^{2/5} \gamma_m^{-8/5} \Gamma^{9/5}$  Hz, where  $l$  and  $n$  are the path length and particle density in the comoving frame, respectively, and we have assumed an electron energy distribution index  $p = 2$ . (We have also assumed an isotropic distribution of electron pitch angles; for a small pitch-angle distribution, the  $\nu^{-2/3}$  portion in eq. [4] would be replaced by  $\nu^0$ .) For  $\nu_a > \nu_m$ , we just have one break at  $\nu_a$  with a low-energy photon index of  $\alpha = 3/2$  (in both the isotropic and small pitch-angle cases). The possibility of self-absorption in GRBs is a controversial issue. We have shown (LP00) that there are bursts for which a self-absorbed spectrum is a better fit than an optically thin one. We also found that in these cases, the absorption frequency

tends to be near the lower edge of the BATSE window. In addition to this, Strohmayer et al. (1998) found that a number of bursts observed by *Ginga* with values of  $E_p$  in the range 2–100 keV have steep ( $\alpha \sim 1$ ) low-energy spectral indices consistent with a self-absorbed spectrum. This raises interesting questions about the physics of the ambient plasma because self-absorption in a GRB requires fairly large magnetic fields and particle densities. For example, if the absorption frequency is less than the minimum electron frequency, the optical depth to synchrotron self-absorption is

$$\tau \sim (l/10^{13} \text{ cm})(n/10^8 \text{ cm}^{-3})(B/10^8 \text{ G})^{2/3}(\gamma_m/50)^{-8/3} \\ \times (\Gamma/10^3)^3(h\nu_{\text{obs}}/40 \text{ keV})^{-5/3}(1+z)^{-5/3}, \quad (5)$$

where  $\nu_{\text{obs}}$  is the absorption frequency in the observer's frame and  $z$  is the redshift of the GRB. Note that this frequency falls within BATSE's spectral window under certain, perhaps somewhat extreme, conditions. The physical processes required to achieve these conditions will need to be theoretically established if the data prove self-absorption to be a viable model. We point out that the next generation of GRB-dedicated telescopes—namely, *Swift* and the *High Energy Transient Explorer 2 (HETE-2)*—will obtain more spectral data in energy ranges lower than the BATSE threshold (of about 25 keV) and can firmly establish the presence or absence of a self-absorbed portion of the low-energy spectrum.

Figure 1 shows the various spectra for the different emission regimes. Note that we have plotted the  $F_\nu$  spectrum rather than  $F_\gamma = F_\nu/\nu$  to emphasize the differences in the

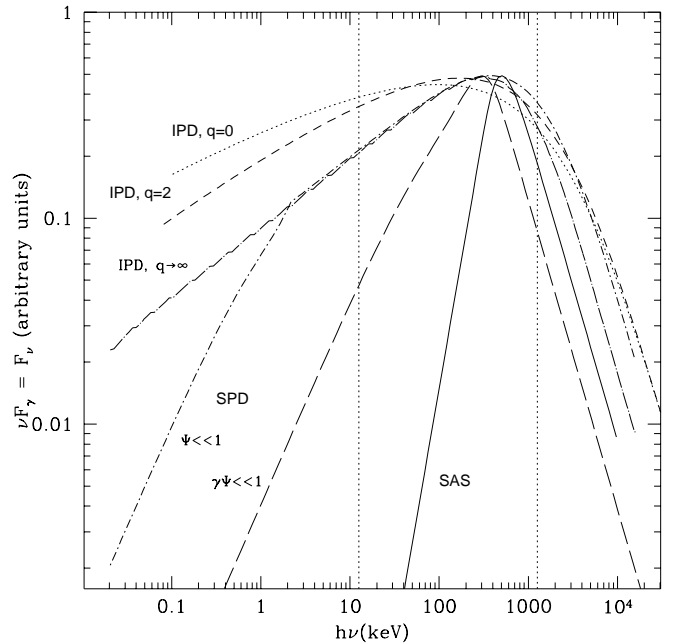


FIG. 1.—Various synchrotron energy spectra  $F_\nu$  (in arbitrary units) as a function of energy  $h\nu$  in keV. The dot-dashed line is optically thin radiation from an isotropic distribution of electrons with a sharp minimum energy cutoff, while the dotted and short-dashed lines show the IPD synchrotron spectra for smooth cutoffs to the electron distribution ( $q = 0$  and  $q = 2$ , respectively). Note that for finite values of  $q$ , the asymptotic  $\nu^{1/3}$  spectrum is achieved at photon energies much lower than  $E_p$ . The solid line shows a self-absorbed spectrum for  $\nu_a > \nu_m$ . The long-dashed and dot-dashed lines indicate the SPD case for small ( $\Psi \ll 1$ ) and very small ( $\gamma\Psi \ll 1$ ) pitch angles, respectively. The vertical lines mark the approximate width of the BATSE spectral window.

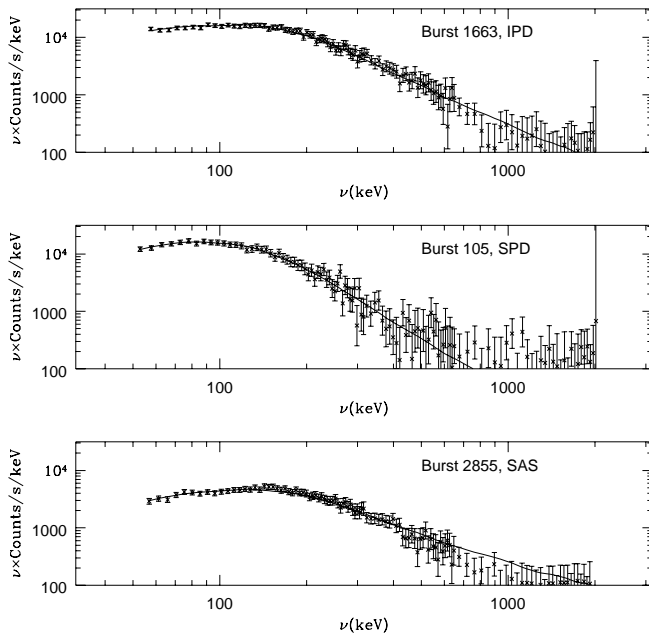


FIG. 2.—Fits to the three different synchrotron models described in § 2. The emission regime that best fits each burst (indicated in each figure) is the regime inferred from the Band fit value of  $\alpha$  at the time of each spectrum. (Note that these are the actual counts spectra of the burst, which is the photon spectrum convolved with the detector response matrix.)

various low-energy slopes of the spectra between the different emission regimes. Throughout the rest of the paper, we use the value of the low-energy photon index  $\alpha$  to distinguish between the different emission scenarios, where the *IPD* case is defined by  $\alpha \lesssim -\frac{2}{3}$ , *SPD* by  $-\frac{2}{3} \lesssim \alpha \lesssim 0$ , and *SAS* by  $\alpha \gtrsim 0$ .

#### 2.4. Spectral Fits: Directly Testing the Model

To test how well these synchrotron models actually describe the existing data, we have performed time-resolved spectral fits to a sample of data from the BATSE archive. We use 128 channel, 128 ms time-resolved HER data, which are obtained for the most brightly illuminated of the eight detectors from the on-line archive.<sup>3</sup> We plot the total counts as a function of time (the burst time profile) summing over all energy bins; from this, we pick out time intervals for the background and over which to do our spectral fits. We then subtract off the background counts averaged over our specified “background” time intervals from our raw spectral counts data for each energy bin (the alternative method of subtracting a fitted background photon model off of the spectral photon model is mathematically equivalent—that is, it is equivalent to subtract off the background before convolving with the detector response matrix [DRM] or after convolving with the DRM). We then fit our photon models to the data by convolving them with the DRM to get model counts and then minimized  $\chi^2 = (\text{data} - \text{model counts})^2 / \sigma^2$  via a downhill simplex method.

Our models are described in detail in LP00 and briefly above. We fit each spectrum to all three emission scenarios and then evaluate the fits based on their values of a reduced  $\chi^2$ . In Figure 2, we show examples of spectral fits in each emission regime. Each fit is taken at a time during the burst

spectral evolution when the  $\alpha$  parameter corresponded to the respective model. For example, in the top panel—burst 1663—the spectrum is from a time when  $\alpha \sim -\frac{2}{3}$ , while in the middle panel—burst 105—the spectrum is from a time in the profile when  $\alpha = 0$ . Similarly, for the bottom panel, this spectrum corresponds to a time when  $\alpha = 1$ . The reduced  $\chi^2$  are 0.34, 0.33, and 0.50 for the top, middle, and bottom panels, respectively. In general the best model turns out to correspond to the emission regime suggested by Band’s  $\alpha$ -values, which confirms our proposed method of physically interpreting Band fits based on the bursts’ low-energy photon index (for example, an IPD fit to the spectrum of burst 105 gave a  $\chi^2 > 1$  compared to the  $\chi^2 = 0.33$  for an SPD fit). However, we have not yet been able to confirm this for the self-absorbed case; although in some bursts the SAS was clearly better than the IPD case, SPD seemed to do statistically as well for the small sample of bursts that we have tried. As mentioned above, better low-energy data is needed to definitively establish the existence of a self-absorbed component in some GRB spectra. Nonetheless, in this paper, we interpret those bursts with a low-energy photon index larger than the SPD limit of  $\alpha = 0$  as SAS cases.

### 3. EXPECTED CORRELATIONS AMONG SPECTRAL PARAMETERS

Ideally, we would like to carry out such fits to a large sample of bursts and characterize the physics of each burst as well as trends among large samples of bursts directly through the physical parameters yielded by the fits. However, this is a large and time-consuming task, and in fact, we can learn a great deal about the underlying physics of GRBs through an analysis of the phenomenological spectral parameters in terms of a physical model. We have already shown that the Band parameter  $\alpha$  is a good indication of the relevant synchrotron emission regime (IPD, SPD, or SAS). Examining correlations among the various Band parameters can lead to additional insights into the physics governing the emission when interpreted in the context of a physical model. Below we discuss the types of correlations one might expect among the Band spectral parameters for the different emission scenarios described above. In §§ 4 and 5, we compare these correlations with what we find in the GRB data.

#### 3.1. $\alpha$ - $E_p$ Correlation

Two different correlations are expected for these parameters:

1. We expect a positive correlation between  $E_p$  and  $\alpha$  because of the instrumental effect described in LP00. If  $E_p$  is close to the edge of the BATSE window, the low-energy photon index may not yet have reached its asymptotic value, and a smaller (or softer) value of  $\alpha$  (relative to the asymptotic value) will be determined. A smooth cutoff to the electron energy distribution will exacerbate this effect because for a smoother cutoff (or a lower  $q$ ), the low-energy asymptote is reached farther away from  $E_p$ , nearer to (or even below) the low-energy edge of the detector spectral window. Note that a dispersion in the smoothness of the low-energy cutoff will tend to wash this correlation out to some degree, as seen in Figure 4 of LP00. For the cases of small pitch-angle radiation and the self-absorbed spectrum, this effect will be weaker because the low-energy asymptotes

<sup>3</sup> Available at <ftp://cosscc.gsfc.nasa.gov/compton/data/batse/trigger>.

are reached more quickly (i.e., at energies closer to  $E_p$ ) than for the isotropic optically thin case (see Fig. 1).

2. We also expect evidence of a negative correlation between  $E_p$  and  $\alpha$  as we transition from the IPD to the SPD regime, i.e., for  $-\frac{2}{3} < \alpha < 0$ . In this case, the pitch angle decreases so that  $E_p \propto \sin \Psi$  decreases if all other physical parameters ( $B$  and  $\gamma_m$ ) remain constant. In addition, as we go from the small pitch-angle regime,  $\Psi \gamma_m \sim 1$  ( $\Psi \ll 1$ ), to the very small pitch-angle regime, to  $\Psi \gamma_m \ll 1$ , the  $\nu^{-2/3}$  portion of the spectrum disappears, and we are left with only the  $\nu^0$  portion. In other words, as the mean of the pitch-angle distribution decreases to very small values,  $E_p$  decreases, and the value of  $\alpha$  decreases from  $-\frac{2}{3}$  to 0. This negative correlation will compete with the positive instrumental correlation mentioned above.

### 3.2. $\beta$ - $E_p$ Correlation

We expect a similar correlation between  $E_p$  and  $\beta$  because of the instrumental effects. A dispersion in the high-energy electron index  $p$  will tend to reduce this correlation. However, in practice—partly because the high-energy spectral data are not very constraining and partly because  $E_p$  is usually well below the upper edge of the BATSE window (about 1.5 MeV) for those bursts with spectral fits—this correlation between  $E_p$  and  $\beta$  is not evident in the data. For a few sample spectra, we find that  $E_p$  has to be greater than around 1100 keV before  $\beta$  is affected by this instrumental effect.

### 3.3. Total Flux- $E_p$ Correlation

We might expect a positive correlation between  $E_p$  and the flux of the burst. If  $E_p$  changes because of either a change in the magnetic field or  $\gamma_m$ , then the flux, which also depends on positive powers of both of these parameters, will also increase (Pacholczyk 1970). This effect of course will be weakened to some degree by the distribution of redshifts of GRBs (if we examine the whole spectral sample instead of one burst). However, as shown in Lloyd, Petrosian, & Mallozzi (2000), the cosmological contribution to such a correlation (higher redshift reduces the observed value of  $E_p$  and flux for a given burst) is negligible because of the large intrinsic dispersion in the luminosity function and intrinsic  $E_p$  distribution, so that any correlation we do observe can be attributed to an intrinsic effect.

## 4. THE TIME-RESOLVED SPECTRAL DATA: GLOBAL BEHAVIOR

We showed in LP00 that the time-averaged spectral parameter distributions are consistent with the models of synchrotron emission described above. We also showed for several GRBs that the evolution of different spectral parameters of a particular burst track each other throughout their time evolution in a way that is easily interpreted in our models. We want to test our models and, in particular, investigate the latter point in more detail by examining the behavior of a large sample of *time-resolved* spectral parameters. The ideal is to learn something about how the plasma parameters are changing between emission episodes in a burst by examining the time-resolved Band spectral parameters in the context of our synchrotron models. As mentioned in § 3, because the spectral parameters can depend on more than one physical quantity, we look for *correlations between the spectral parameters* (rather than

examining the evolution of one spectral parameter in time) in order to break some of the degeneracies in interpreting the evolution of the physical parameters.

One way to do this is to look for particular trends between pulses within individual bursts. For example, Crider et al. (1997) claim to see a positive correlation between  $E_p$  and  $\alpha$  in 47 individual bursts.<sup>4</sup> The advantage of looking at spectral evolution within individual bursts is that correlations between the spectra do not contain any dispersions or contributions that might arise because of redshift effects. However, looking for global evolutionary trends in the data by examining individual bursts is a difficult and challenging task, particularly when we differentiate between different emission regimes. This is not only because there is a small number (typically  $\sim 20$ ) of time-resolved spectra per burst but also because there is a small number of points *per emission regime*, particularly for the SPD and SAS regimes. Therefore, attaching a significance to correlations between spectral parameters in different emission regimes for a single burst is, in general, not statistically robust (B. Efron 2000, private communication), and there is therefore no reliable way to compare results with other bursts in order to establish general trends in the evolution.

We would like to investigate if there are any average trends present among the spectral parameters in each emission regime. Although we do examine the behavior of some individual bursts in the next section, this goal is best accomplished by combining all 2026 time-resolved spectra available and searching for any global trends in this sample. Trends present in this entire sample will reflect the trends of temporal behavior in individual bursts on average and can therefore help us gain insight into the evolutionary trends present in individual bursts. We can then test whether these trends are consistent with our models of synchrotron emission and—if so—ideally learn something about the evolution of the physical conditions (such as the magnetic field and Lorentz factors) throughout a GRB.

### 4.1. Data and the $\alpha$ -Distribution

Our data is taken from the catalog of Preece et al. (2000), which contains high energy resolution, time-resolved spectral fits to a large number of BATSE bursts (see their paper for discussion of data type, time, and energy resolution, etc.). Our sample consists of individual spectra for which the HER data type is used in the spectral fit (because of its superior energy resolution; see Preece et al. 2000 for description of data types) and for which the Band function provided a reliable fit in the  $\sim 20$  keV to  $\sim 1.5$  MeV range. These criteria leave us with 2051 spectra. We then eliminate 25 additional individual spectra because the error bars on the spectral parameters are 0, indicating an error in the fitting procedure. This leaves us with 2026 spectra; although this is only a fraction of the  $\sim 5000$  spectra in the Preece catalog, we believe it is an accurate representation of at least those bursts that are described by the Band spectrum, and as discussed in Preece et al. (2000), this spectral form describes the large majority of bursts very well (see

<sup>4</sup> We note that they do not distinguish between different emission regimes in their analysis. They have also found evidence for a negative correlation in some individual bursts, but with admittedly low statistical significance. They do not report the  $\alpha$ -values for these bursts (so that they might be interpreted in terms of a particular “emission regime” of our models).

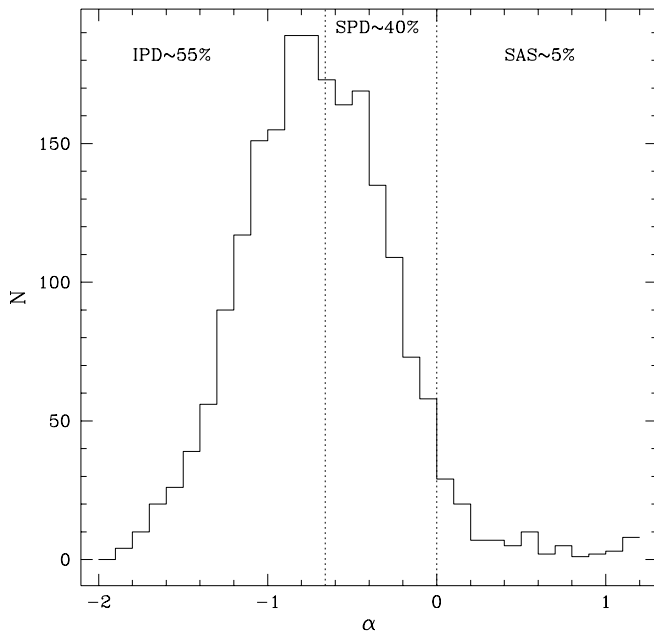


FIG. 3.—Histogram of low-energy photon index  $\alpha$ , a compilation of 2026 time-resolved spectral fits from Preece et al. (2000). The different emission regimes and percent of spectra in each regime are marked on the figure.

also Band et al. 1993; Mallozzi et al. 1996; Lloyd & Petrosian 1999).<sup>5</sup>

#### 4.1.1. The $\alpha$ -Distribution

As discussed in § 2, the parameter  $\alpha$  is the best parameter for distinguishing between the various synchrotron regimes. Figure 3 shows a histogram of  $\alpha$  (taken from the 2026 time-resolved fits of Preece et al. 2000) with each regime clearly marked.<sup>6</sup> For our sample, we find the percent of spectra in each regime is as shown in Table 1.

Note that there are a significant number of spectra in the SPD and SAS regime. It is important, however, to briefly discuss how the error bars on the parameter  $\alpha$  affect the

<sup>5</sup> For some bursts, however, this is not the case. For example, Preece et al. (1996) showed that in a sample of about 90 *time-averaged* spectra, about 14% showed an X-ray excess in the 7–20 keV range. Strohmayer et al. (1998) also found an X-ray excess in at least one *Ginga* burst. Such an excess would tend to affect the low-energy photon index—giving a softer (lower) value of  $\alpha$  than if there were no excess. This, in turn, would add some scatter to the expected correlations between  $\alpha$  and  $E_p$  discussed in § 3.1. However, because we are looking at the subset of data for which the Band spectrum provides a reliable fit and we are examining *time-resolved* spectra between 20 and 1500 keV (above the range in which these excesses have been found), we do not expect that this would significantly affect our results. Of course, one can always add additional emission components to any model, but because we have no evidence of it in our data, we take the simplest interpretation of a single-component emission model and see what we can learn from the data under this assumption.

<sup>6</sup> We point out that the peak of this distribution falls just slightly higher than the  $\alpha$ -distribution presented in Preece et al. 2000, which peaked at around  $-1$ . This may be partly due to the differences in the way we binned our data, but it primarily reflects the fact that we have only included those bursts with Band fits in our sample; for example, bursts that are described well by a “Comptonized” spectrum or simple broken power-law spectra tend to have a slightly lower value of  $\alpha$  than those described by the Band spectrum and may shift the peak of the  $\alpha$ -distribution toward lower values. In any case, we note the difference is within the average  $1\sigma$  error on  $\alpha$  ( $\langle\Delta\alpha\rangle \sim 0.28$ ) and remind the reader we are only examining those bursts for which the Band function provided an acceptable spectral fit.

TABLE 1

NUMBER OF TIME-RESOLVED GRB SPECTRA BELONGING TO EACH EMISSION REGIME

Regime	$\alpha$ Range	Number in Regime	Percent in Regime
IPD .....	$\alpha \leq -\frac{2}{3}$	1122	55
SPD .....	$-\frac{2}{3} < \alpha \leq 0$	805	40
SAS .....	$0 < \alpha < 3/2$	99	5

interpretation of this distribution. First, we point out that Preece et al. (2000) showed that the error bar on  $\alpha$  cannot alone account for the large dispersion in the distribution. In our sample, we find that the average  $1\sigma$  error on  $\alpha$  is  $\langle\Delta\alpha\rangle \sim 0.28$ , suggesting (in agreement with the more detailed analysis of Preece et al.) that there is still a significant number of bursts above the line of death  $\alpha = -\frac{2}{3}$ . To quantify this, we have computed the number of bursts in each emission regime using the upper and lower  $1\sigma$  limits of  $\alpha$ . If we take all values of  $\alpha$  at their upper limits ( $\alpha + \Delta\alpha$ ), we find 42%, 46%, and 12% of bursts in the IPD, SPD, and SAS regimes, respectively. Taking all values of  $\alpha$  at their  $1\sigma$  lower limits ( $\alpha - \Delta\alpha$ ), we find 69%, 29%, and 2% of bursts in the IPD, SPD, and SAS regimes, respectively. Although the error bars on  $\alpha$  can make some difference as to the numbers of spectra in each regime, we will see that this does not affect the qualitative nature of our conclusions below. We now discuss the correlations present in the data and their consistency with what we expect in the context of the three synchrotron emission scenarios.

#### 4.2. Observed $\alpha$ - $E_p$ Correlation

Figures 4a and 4b show the binned average correlation between  $E_p$  and  $\alpha$  present in the time-resolved data. For each of these figures, we have sorted  $\alpha$  in ascending order and binned the data every 100 points (the horizontal error bars indicate the size of the bins). We then computed the average and median  $E_p$  for these 100 points. In Figure 4a, we show the average  $\bar{E}_p$  versus  $\alpha$ , where the vertical error bars are simply the variance of the mean value of  $E_p$ ; in Figure 4b, we have plotted the median  $E_p$ , where the solid and dotted vertical error bars indicate the range of  $E_p$  about the *median* value that includes 68% and 90% of the data, respectively (we do point out that the scatter of  $E_p$  in each bin is not necessarily Gaussian; see, e.g., Preece et al. 1996, 1998a). The observed trends are consistent with what is expected from our model in each emission scenario and tell us something important about the role various effects play in the correlations, as we discuss below.

##### 4.2.1. IPD Regime

Performing a Kendall’s  $\tau$ -test on all of the (unbinned) data, we find a  $9\sigma$  positive correlation between  $\alpha$  and  $E_p$  in the IPD regime. To account for both the error in  $\alpha$  and  $E_p$ , we have performed this test on all permutations of correlations between the lower and upper values of  $\alpha$  (from the  $1\sigma$  error bars) with the lower and upper values of  $E_p$ . In addition, we have averaged the value of  $\tau$  from 100 sets of data, in which—for each data point— $\alpha$  and  $E_p$  are drawn from Gaussian distributions with means equal to the parameter values given in the catalog and standard deviations corresponding to the error bars. *In all cases, we find a highly significant ( $>6\sigma$ ) correlation.* The positive correlation between  $\alpha$  and  $E_p$  in the IPD regime can be simply

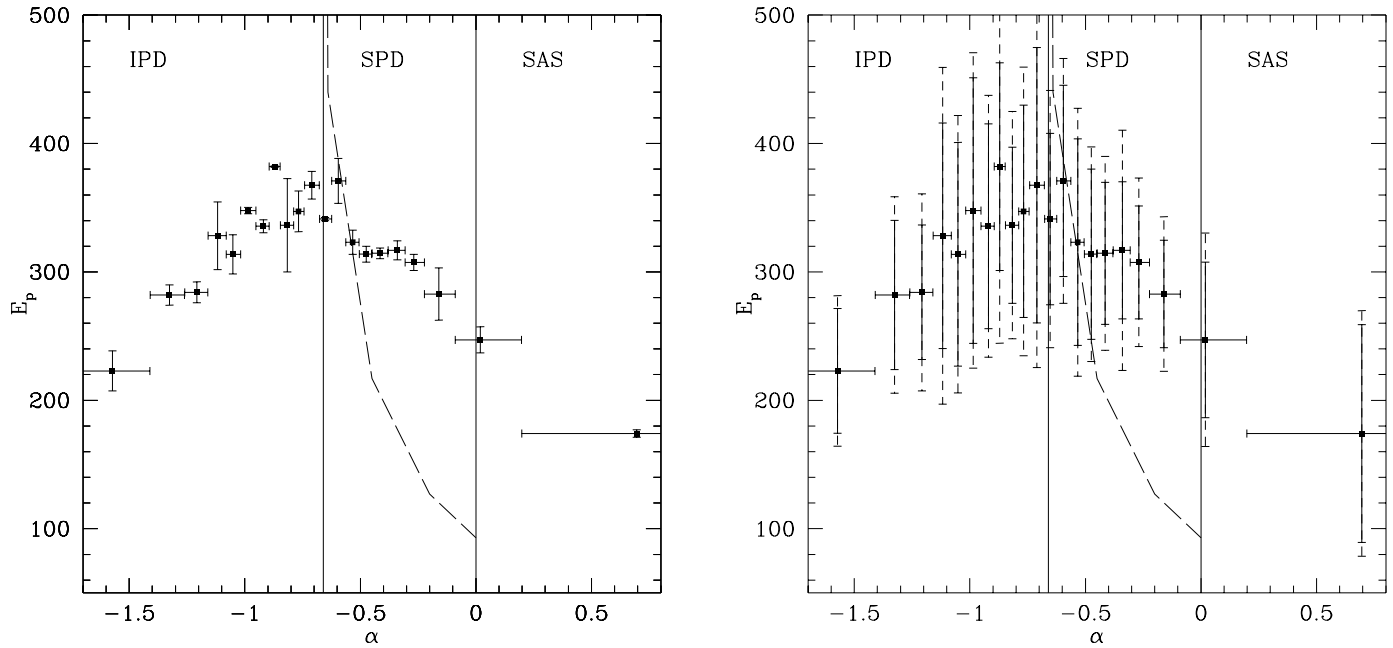


FIG. 4.—Peak of  $\nu F_\nu$  spectrum  $E_p$  vs. low-energy index  $\alpha$  for binned 2026 time-resolved spectral fits. The left-hand panel plots the variance of the average  $E_p$  as the vertical error bars, while the right-hand panel plots the median values of  $E_p$  and the range that contains 68% (solid lines) and 90% (dotted lines) of the data around the median. Each regime of emission is marked on the plot. The dashed line in the SPD regime is an example of how  $E_p$  changes as a function of  $\alpha$  within the BATSE spectral window as the mean of the electron pitch angle decreases, but all other parameters ( $B$ ,  $\gamma_m$ ,  $p$ ,  $q$ ) remain constant.

understood by the instrumental effect discussed in § 3. However, for a given value of the low-energy electron distribution cutoff parameter  $q$ , the correlation is expected to be much stronger than observed (see Fig. 4 of LP00). Of course, any dispersion in  $q$  will tend to weaken and flatten this correlation. In fact, we can give a rough but quantitative estimate of the  $q$  distribution required to produce the observed  $E_p$ - $\alpha$  correlation seen in Figure 4. For each burst (under the assumption that optically thin synchrotron emission from an isotropic distribution of electrons produces its spectrum), we can estimate the  $q$ -value necessary to produce the burst's  $E_p$ - and  $\alpha$ -values, simply from the determined relationships between  $\alpha$  and  $E_p$  for different values of  $q$  in Figure 4 of LP00. In Figure 5, we present an estimate of the distribution of  $q$  required to reproduce the data and therefore the shallow correlation between  $\alpha$  and  $E_p$  observed in the IPD regime. Note that the dotted part of the histogram is not at all well constrained because the correlation dramatically weakens for very high values of  $q$ , and the solutions become quite degenerate (that is, for a given  $E_p$ , a  $q$  of 5 or 10 may produce the same value of  $\alpha$ ).

#### 4.2.2. SPD Regime

The sign of the correlation between  $\alpha$  and  $E_p$  reverses for values of  $\alpha \gtrsim -0.7$ , which is suggestively very close to where we expect a transition from the IPD to SPD regime. Performing a Kendall's  $\tau$ -test on all of the (unbinned) data in this regime, we find a  $4\sigma$  negative correlation between  $\alpha$  and  $E_p$ . Again, to account for the error in both  $\alpha$  and  $E_p$ , we have performed this test on all permutations of correlations between the lower and upper values of  $\alpha$  (from the  $1\sigma$  error bars) with the lower and upper values of  $E_p$  as well as averaged the  $\tau$ -value from 100 sets of data drawn from distributions based on the existing data, according to the prescription described in § 4.2.1. In all of these cases, we find a significant ( $> 3\sigma$ ) negative correlation. As mentioned in § 3,

this type of correlation is natural in the small pitch-angle regime simply as a result of decreasing average pitch angle. As seen in equation (2) and described in § 3.1, when  $\Psi$  decreases, the characteristic SPD frequency  $\nu_s$  approaches the characteristic IPD frequency  $\nu_m$  causing the fitted value of  $\alpha$  to increase from  $-\frac{2}{3}$  to 0. Meanwhile,  $E_p \propto \nu_m \propto \sin \Psi$

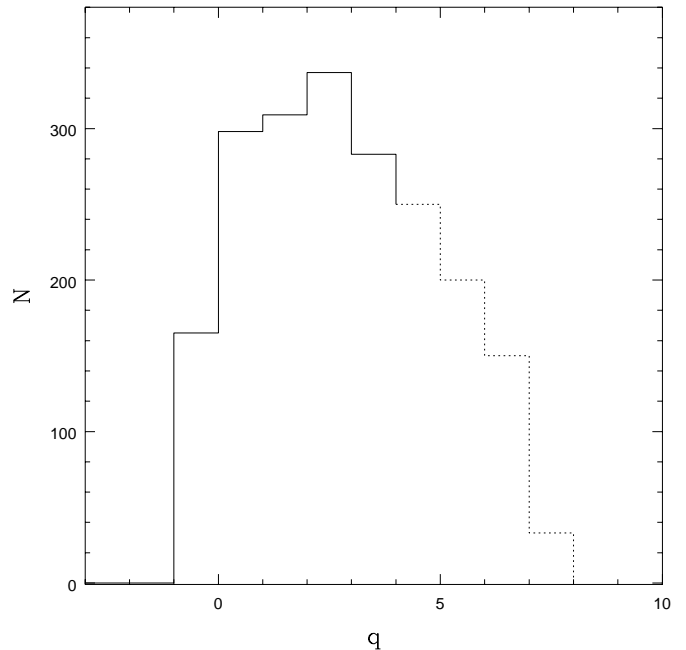


FIG. 5.—Estimated distribution of  $q$ , given the observed correlation between  $\alpha$  and  $E_p$  in the IPD regime. There is a degeneracy among high values of  $q$  (that is, for different values of  $q \geq 5$ , we obtain the same observed  $\alpha$ -value for a given  $E_p$ ); the dotted portion of the histogram attempts to account for this degeneracy and is simply a reasonable guess at how this portion of the histogram behaves.

will decrease as the pitch-angle decreases. We believe this physical effect produces the negative correlation seen in Figure 4 and dominates over the positive instrumental correlation between  $\alpha$  and  $E_p$ . (The instrumental effect is lessened in this regime because of the steeper low-energy slope [relative to the isotropic case], which allows the spectrum to reach its low-energy asymptote more quickly.) We point out, however, that the quantitative value of the slope is somewhat shallower than what is naively expected if *only* the mean value of the pitch angle  $\Psi$  changes, while all other parameters remain constant. This is illustrated by the dashed line in Figure 4, which shows how  $E_p$  changes as a function of  $\alpha$  as the pitch angle  $\Psi$  decreases. To obtain this curve, we simulate SPD spectra for a series of decreasing pitch angles (given a constant magnetic field  $\gamma_m$  and bulk Lorentz factor  $\Gamma$ ), add Poisson noise to the spectra, and then fit a Band spectrum to each curve; this gives us values for  $E_p$  and  $\alpha$  as a function of decreasing pitch angle. Naturally, dispersion in the magnetic field  $\gamma_m$  or a bulk Lorentz factor will tend to weaken the correlation (as is observed). We discuss this further in § 4.2.4.

#### 4.2.3. SAS Regime

This negative correlation appears to continue for the self-absorbed spectra (SAS). The low  $E_p$ -value in the SAS regime is consistent with our suggestion (LP00) that the self-absorption frequency is at the lower edge of the BATSE window (around 50 keV). However, there are few bursts in this regime, and this may be a result of an observational selection effect. For very large values of  $\alpha$ , bursts with lower values of  $E_p$  (everything else being equal) will have a better chance of triggering the BATSE detector. Unfortunately, there is not yet sufficient data to test this conjecture. We note that such a selection effect does *not* seem likely to explain the negative correlation in the SPD regime because of the small difference in the  $E_p$  distribution between the IPD ( $\alpha \lesssim -0.7$ ) and SPD ( $\alpha \gtrsim -0.7$ ) cases, as shown in Figure 6.

#### 4.2.4. Summary

The  $\alpha$ - $E_p$  correlations provide, at least qualitatively, further support for the synchrotron model and possibly the small pitch-angle distribution (SPD) scenario. Our most intriguing result is that at  $\alpha \gtrsim -0.7$ , the  $\alpha$ - $E_p$  correlation goes from positive (as expected purely from instrumental effects discussed above and in LP00) to negative. This negative correlation is a natural expectation in the SPD emission regime of our synchrotron models. However, there are some interesting quantitative points to address. The dashed line in Figure 4 gives an example of how  $E_p$  should change as a function of  $\alpha$  in the BATSE spectral window if only the mean of the electron pitch angle  $\Psi$  changes (all other parameters such as  $B$  and  $\gamma_m$  remaining constant). The parameter  $E_p$ —in going from the isotropic to anisotropic electron distribution regime—should decrease by a factor  $\sim \gamma_m/2$  as  $\sin \Psi$  decreases from  $\sim 1$  to  $\sim 1/\gamma_m$  (see eqs. [2] and [3]). It is often assumed that the electron Lorentz factors in GRBs are  $\sim 100$ —approximately equal to the bulk Lorentz factors, which need to be at least this large to keep the medium optically thin to pair production and inverse Compton scattering (see Lithwick & Sari 2001 for a recent discussion of this issue). In these cases, we should see a decrease in  $E_p$  by a factor  $\sim 50$  as we transition from the isotropic to the very small pitch-angle regime. Although this

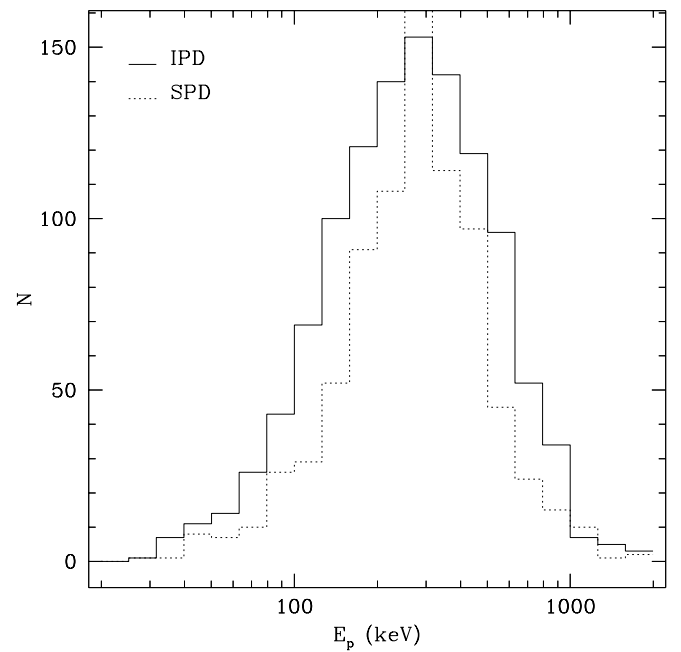


FIG. 6.— $E_p$  distribution for those GRBs in the IPD regime (solid line) and SPD regime (dotted line).

strong negative correlation will be weakened to some degree because of dispersion in the intrinsic values of  $\Psi$  and  $\gamma_m$  as well as variation in the magnetic field, we might expect a stronger decrease in  $E_p$  than what is seen in the data for the large values of  $\gamma_m$  mentioned above. The relatively small observed change in  $E_p$  could mean several things: (1) The minimum electron Lorentz factor or the magnetic field of the electrons *increases* as we transition to a physical regime in which electrons are accelerated primarily along the magnetic field lines. This may be a very plausible explanation—there may exist physical situations that require either a higher magnetic field or characteristic electron Lorentz factor, in which it is very efficient to accelerate along the magnetic field lines. The details of this are beyond the scope of this paper. (2) The electron Lorentz factors could be much smaller than 100—in fact, in an internal shocks model, it is expected that the electron Lorentz factors will be on the order of the relative Lorentz factor of the two shells, which can be on the order of a few (Piran 1999). This would be consistent with the relatively small decrease in  $E_p$  in the SPD regime, seen in the data. We caution, however, that with electron Lorentz factors so low, we require a larger value of the  $B$  field (for a given observed value of, e.g.,  $E_p$ ), and in addition, some of the assumptions implicit in our spectral models (e.g., extreme relativistic velocities) may not hold. (3) This model is incorrect, and an alternative explanation is needed to accommodate bursts above the  $\alpha = -\frac{2}{3}$  line of death. For example, the photon indices  $\alpha$  between  $-\frac{2}{3}$  and the self-absorption value of 1 may simply be due to the presence of *both* the absorption frequency and minimum electron frequency present in the BATSE window. As long as  $v_m > v_a$  and spectral fits place the characteristic break energy at  $E_p \propto v_m$ , then the low-energy photon index will be a weighted average of  $-\frac{2}{3}$  and 1 (depending on the relative values of  $v_m$  and  $v_a$ ). We might then explain the observed negative correlation between  $\alpha$  and  $E_p$  for  $-\frac{2}{3} \lesssim \alpha \lesssim 0$  by the following: As  $v_m$  decreases (while  $v_a$  remains roughly



constant or even increases),  $E_p$  decreases, and we get less of the  $-\frac{2}{3}$  portion of the spectrum relative to the slope = 1 portion. This will cause the value of  $\alpha$  to increase relative to the  $-\frac{2}{3}$  value (of course, in this case, we expect that the Band fits with a single break will not be as good). We do not go into further detail on this subject and only present it as another possibility.

#### 4.3. Observed Total Photon Flux– $E_p$ Correlation

Figure 7 shows a correlation between the average burst total peak flux and  $E_p$  (we point out that this correlation is also present between the normalization or height of the spectrum and  $E_p$ , so that the value of the peak flux is not greatly affected by the values of the low- and high-energy spectral indices and is more a measure of the brightness or overall emission power). The correlation is well established and has also been reported within individual bursts (Mazets et al. 2002). This correlation can be due to several effects in a synchrotron model including increasing magnetic field, minimum electron Lorentz factor  $\gamma_m$ , and/or bulk Lorentz factor  $\Gamma$ ; in Figure 7, we show  $f_\gamma$  as a function of  $E_p$  in an IPD regime for a changing magnetic field (*dotted line*) and minimum electron Lorentz factor (*dashed line*). We point out again, however, that the theoretical lines describe the relation between luminosity and the value of  $E_p$  in the cosmological rest frame of the burst. A dispersion in the redshift distribution of the GRBs will tend to smear out this theoretical correlation. We interpret this correlation as a relation between  $E_p$  and flux from pulse to pulse (or emission episode to emission episode) and have suggested ways to reproduce this by varying the plasma parameters in the context of synchrotron radiation. We note that such a correlation has been reported in the decay phase of individual pulses of bursts (see, e.g., Borgonovo & Ryde 2001; Ryde & Svensson 2002). Such a correlation in a single pulse may arise from a change in plasma parameters *within* a single

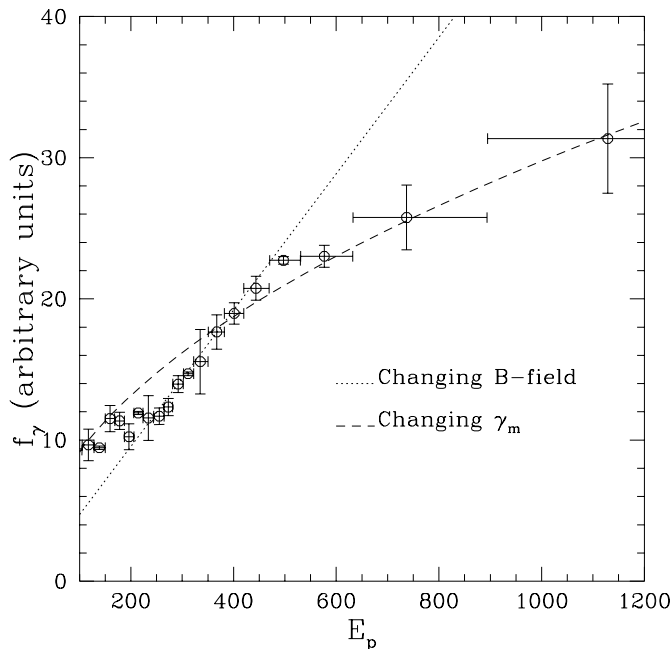


FIG. 7.—Photon flux  $f_\gamma$  vs.  $E_p$  for the binned 2026 spectra in our sample. The dotted line shows the correlation (for all bursts at the same redshift) as a function of an increasing  $B$  field. The dashed line shows  $f_\gamma$  vs.  $E_p$  as  $\gamma_m$  increases.

emission episode but can also be produced by relativistic beaming effects alone (photons from the edge of the beaming cone arrive later than those from the middle of the cone; the edge photons have a smaller Doppler factor [by  $1/\Gamma^2$ ] and so have both a smaller value of flux *and*  $E_p$  at later times in the pulse). In any case, the above synchrotron interpretation appears as a plausible candidate for the description of the correlation observed in the data.

There may be correlations as a result of other physical effects and correlations between the physical parameters themselves. For example, if the particle number was conserved in an emission episode, then the normalization of the particle distribution would increase as  $q$  increased—this would cause an increase in the overall normalization of the spectrum; since the total particle number  $\int N(\gamma)d\gamma = \int N_0 \{(\gamma/\gamma_m)^q / [1 + (\gamma/\gamma_m)^{p+q}]\} d\gamma$ , then  $N_0$  scales roughly linearly with  $q$ .

#### 5. EXAMPLES OF SPECTRAL EVOLUTION IN INDIVIDUAL BURSTS

Because each pulse is a separate emission episode in our model, it is useful to examine what our models can tell us about the specific behavior of different internal shocks within an individual burst. This section is intended primarily to give the reader a feel for the different types of spectral evolution present in GRBs. All of the following spectral fits are again taken from the catalog of Preece et al. (2000). In Figures 8–13, we display the total photon flux  $f_\gamma$  (*top panels*), the peak of the  $\nu F_\nu$  spectrum  $E_p$  (*middle panels*), and the low-energy photon index  $\alpha$  (*bottom panels*) as a function of time  $t$  for several GRBs; the dashed histogram superimposed on the  $f_\gamma(t)$  plot is the time profile (of detector counts) of the burst. We now qualitatively discuss the behavior in the context of our synchrotron emission scenarios as follows:

1. *Burst 3492.*—Figure 8 displays the spectral evolution of burst BATSE trigger number 3492. This is a good example of how  $E_p$  tracks the flux (or counts) of the burst. The parameter  $\alpha$  somewhat tracks  $E_p$  in this case, but there is evidence for a change in this trend, which could be indicative of a change in the lower cutoff parameter  $q$  of the electron spectrum. We note that—according to its value of  $\alpha$ —this burst remains in the IPD regime throughout its duration.

2. *Burst 5567.*—Figure 9 is another example of  $E_p$  tracking the flux and  $\alpha$  tracking  $E_p$ —entirely in the IPD regime.

3. *Burst 2286.*—In Figure 10,  $E_p$  appears to correlate with the flux and begins at low or soft values and ends at higher, harder values (note that the first point in the plot at  $t = 0$  could be indicative of a precursor). This suggests that during the later emission episodes, either the magnetic field or minimum Lorentz factor changed to cause an increase in  $E_p$ . How this is physically achieved is a complicated issue and is related to the level of turbulence and/or the specifics of the particle acceleration mechanism in the shock. The interpretation of spectral evolution in our models gives us a way of directly interpreting how the physics can change from shock episode to shock episode.

4. *Burst 2855.*—In Figure 11, we see that  $\alpha$  evolves from about 1, interpreted as a self-absorbed situation (and note the low value of  $E_p$ ), to about zero, a value appropriate for the small pitch-angle case, and then back to 1 or the self-absorbed regime at the end of the burst (where again  $E_p$  is at

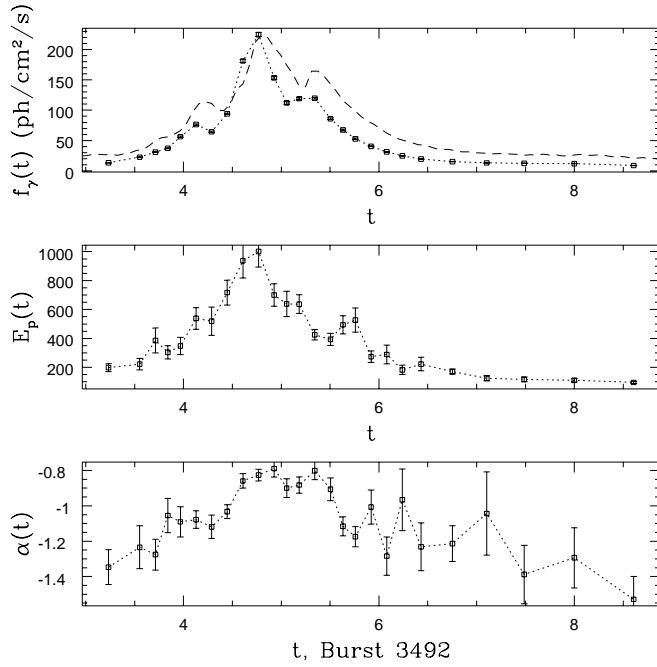


FIG. 8.—Evolution of photon flux  $f_\gamma$  (top),  $E_p$  (middle), and  $\alpha$  (bottom) for burst 3492. The dashed line in the top panel is the total GRB count rate arbitrarily normalized to the peak flux value. Note that this burst remains in the IPD regime throughout.

its lowest). If this interpretation is correct, the physics required to produce this behavior is intriguing to say the least—particularly switching back to the self-absorbed regime at the end of the burst. We also point out that for this burst—which is entirely in the SPD and SAS emission regimes— $\alpha$  appears to roughly anticorrelate with  $E_p$  (see § 3.1 and Fig. 4; although admittedly, the error bars are large here and a constant  $E_p$  is a statistically acceptable—although not the best—description of the data).

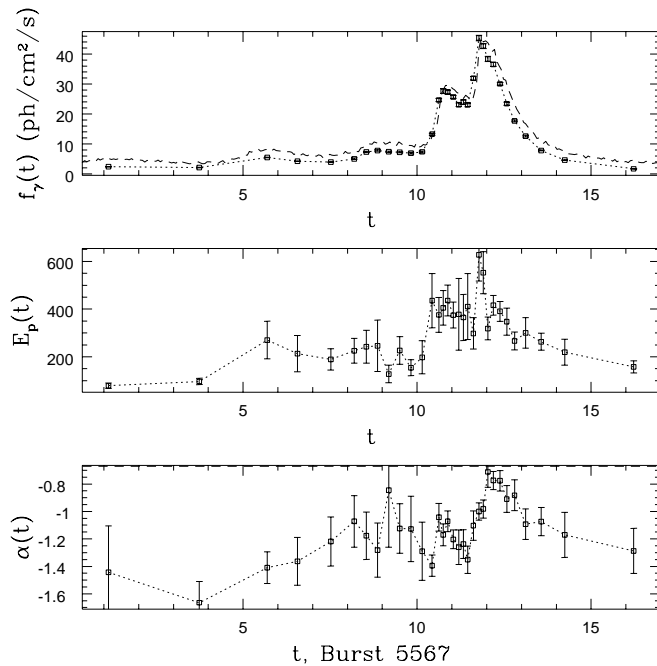


FIG. 9.—Same as Fig. 8, but for burst 5567

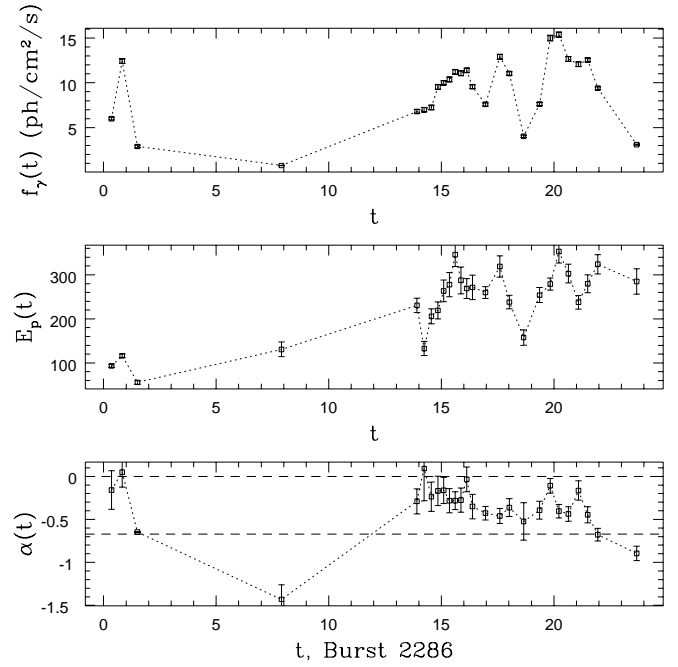


FIG. 10.—Same as Fig. 8, but for burst 2286. In the bottom panel, the upper and lower dashed horizontal lines delineate the SPD and IPD regimes, respectively.

5. *Burst 3489.*—Figure 12 shows an additional example in which  $\alpha$  appears to roughly anticorrelate with  $E_p$  during the various emission episodes of this burst, particularly from  $t \sim 9$  to 14 s.

6. *Burst 1886.*—Figure 13 shows an example of  $\alpha$  transitioning from the SAS to SPD regime; meanwhile,  $E_p$  appears to roughly track the flux of the burst.

The different types of behaviors seen in the individual

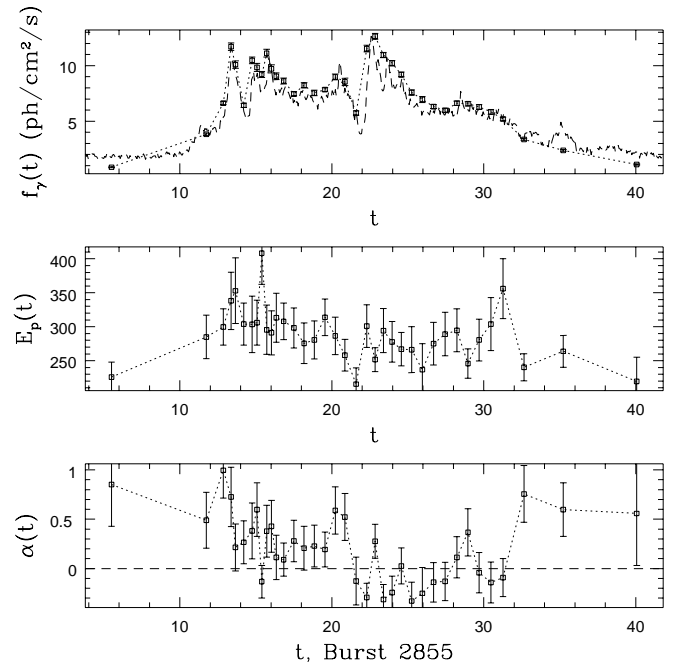


FIG. 11.—Same as Fig. 8, but for burst 2855. The horizontal dashed line separates the SAS (above the line) and SPD (below the line) regimes. Note that this burst remains entirely in the SPD and SAS regimes throughout its entire duration. There is also a rough anticorrelation between  $\alpha$  and  $E_p$  for this burst.

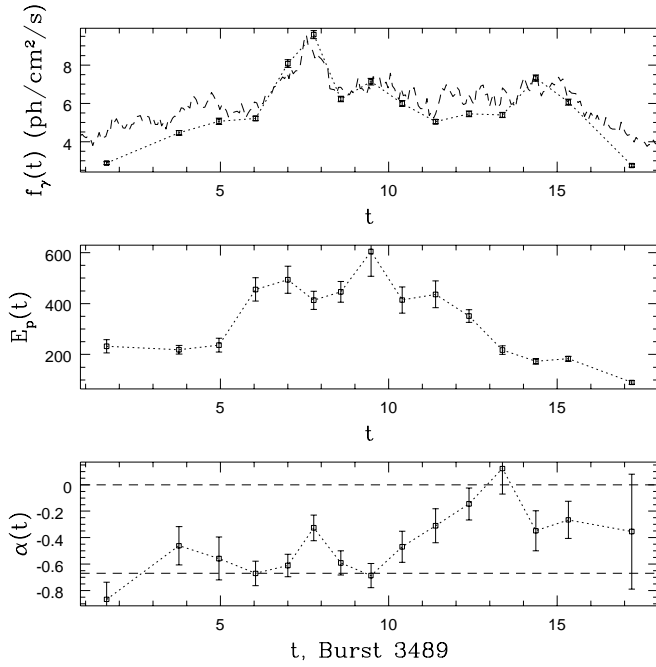


FIG. 12.—Same as Fig. 8, but for burst 3489. During the various emission episodes (to the extent they can be delineated),  $E_p$  is on average lower for the higher values of  $\alpha$  in the SPD regime.

bursts are interesting. On one hand, the spectral evolution appears to be highly varied, and all types of behavior can exist (see also Kargatis et al. 1994). On the other hand, certain trends appear to be present in the data that are at least qualitatively consistent with the global trends presented in § 4. Of course, we acknowledge that these global trends will not be seen in all bursts; establishing statistically

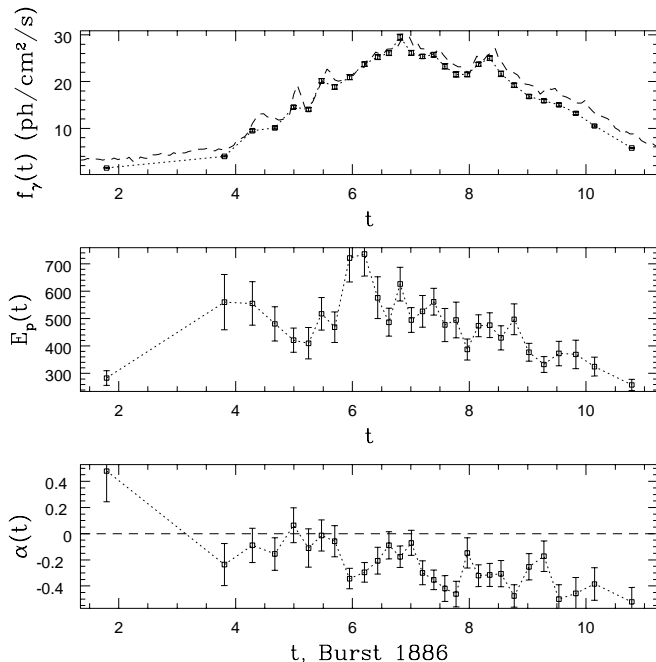


FIG. 13.—Same as Fig. 8, but for burst 1886. The horizontal dashed line delineates the SPD emission regime. This burst evolves from an SAS to SPD regime.

robust trends for each particular emission regime in each particular burst in an attempt to say something about the *average* trends among all bursts is not statistically meaningful (see § 4 for discussion of this issue). We do emphasize again that all types of behavior can occur within individual bursts, and we can use our models to interpret the physics behind any particular evolution. For example, Crider et al. (1997) find that in GRB 910927,<sup>7</sup> there is a positive correlation between  $\alpha$  and  $E_p$  in the SAS regime (and very slightly in the SPD regime, although there are only six points here). This burst appears to have one (or at most, two) smooth, broad pulses, so that there is probably only one (or two) emission episode(s) giving rise to the various spectra. A positive correlation in this case could be due to a number of factors in our model. Of course, as discussed in LP00 and in § 2, the finite bandwidth of the BATSE spectral window will tend to produce a positive correlation between  $\alpha$  and  $E_p$ . However, a physical explanation is also plausible; for example, it is possible that the self-absorbed (or small pitch angle) portion of the spectrum is decreasing relative to the IPD ( $\alpha = -\frac{2}{3}$ ) portion because of a decrease in, say, the magnetic field in the shock. If  $E_p$  corresponded to the self-absorption frequency, this would produce a positive correlation between  $E_p$  and  $\alpha$ . This correlation would be exacerbated if the cutoff to the low end of the electron distribution evolved to a flatter distribution (lower  $q$ -values) throughout the pulse.

Our point is that no matter what the behavior, our models can be used as diagnostics to interpret what types of physical changes may be occurring from pulse to pulse. Note that if we can in fact characterize our synchrotron emission regime by the value of  $\alpha$ , then it is particularly interesting when we see bursts switch emission regimes from pulse to pulse (as a caveat, however, we note that the error bars are significant to some of the spectral fits and that a clear-cut interpretation is not always readily available). This suggests that the fundamental plasma physics (i.e., the particle acceleration) can vary depending on the internal shock conditions within a single burst.

## 6. DISCUSSION AND CONCLUSIONS

In this paper, we have explored the validity of the synchrotron model in explaining the behavior of the time-resolved GRB spectra. In our model, there are three different emission regimes, all distinguished by the value of the low-energy photon index  $\alpha$ . Our model also accounts for the instrumental correlation between  $\alpha$  and  $E_p$  produced when  $E_p$  is near the lower end of the BATSE spectral window (in this case, the spectrum has not reached its low-energy asymptotic value, and so  $\alpha$  will be *softer* or lower for smaller values of  $E_p$ ). In the IPD regime, the synchrotron emission is optically thin from an isotropic electron distribution, and the low-energy photon index  $\alpha$  is less than or equal to  $-\frac{2}{3}$ . In the SPD regime, the emission is primarily from electrons with small pitch angles, and the spectrum consequently has a value of  $\alpha \sim 0$ . Finally, in the SAS regime, the synchrotron photons are self-absorbed, and there is a steep cutoff ( $\alpha = 1$  or  $3/2$  depending on the relative values of the absorption and minimum electron frequency) in the low-energy spectrum.

<sup>7</sup> Note that this burst is not present in the Preece et al. catalog because it does not meet one of the catalog's selection criteria—namely, a peak flux greater than  $10 \text{ photons cm}^{-2} \text{ s}^{-1}$  on the 1024 ms timescale.

We have shown that these models provide an excellent description of the existing data and have presented spectral fits for a few bursts. Our results suggest that the Band parameter  $\alpha$  is a good diagnostic of the relevant emission regime. We also have presented the spectral evolution of the Band spectral parameters (specifically photon flux  $E_p$  and  $\alpha$ ) and interpret the behaviors in the context of our model. We point out that the behavior is quite varied and that there is often evidence that a burst switches emission regimes from pulse to pulse. In attempt to characterize general evolutionary trends exhibited in GRBs, we have combined all 2026 separate time-resolved spectra (from the 80 bursts in our sample) and looked for correlations in this data. Our main results are as follows:

1. We find that the majority of the bursts lie in the IPD regime ( $\sim 55\%$ ) but that a significant fraction of the bursts ( $\sim 40\%$ ) are in the SPD regime. This has interesting implications for the particle acceleration studies in GRBs, as we discuss below. We find that only a small fraction ( $\sim 5\%$ ) of bursts are in the self-absorbed (SAS) regime.

2. We show that there is a strong correlation between  $\alpha$  and  $E_p$  in the IPD regime, which can be attributed to the positive instrumental correlation discussed in LP00. However, there appears to be a negative correlation between  $\alpha$  and  $E_p$  in the SPD regime (albeit, with  $4\sigma$  significance). We interpret this as evidence of the effects of decreasing the electron pitch angle as  $\alpha$  transitions from  $-\frac{2}{3}$  to 0. This physical effect overwhelms the positive instrumental correlation that is dominant in the IPD regime. However, for this physical effect to accommodate the data quantitatively, we need either an increase in the minimum electron Lorentz factor as we transition to the SPD regime or for the absolute value of the electron Lorentz factor to be only on the order of a few. This may very well be the case in an internal shocks model, where the *relative* Lorentz factor of the two shocks is the relevant scale for the electron Lorentz factors.

3. We find a strong positive correlation between the photon flux and  $E_p$ , which can be explained by several effects in a synchrotron emission model. Most notably, a change in the magnetic field or minimum Lorentz factor will produce this type of a correlation.

Our results bring to light the fact that particle acceleration in GRBs is a quite poorly understood problem. Usually, it is assumed that the radiating particles in GRBs are accelerated via repeated scatterings across the (internal) shocks. This is because shocks can quickly accelerate particles to very high energies through repeated scatterings across the shock (the scattering agent being plasma turbulence from, e.g., a two-stream instability [Medvedev & Loeb 1999]). This mechanism, however, predicts several features in the electron distribution not borne out by the data. First, it has been shown (Kirk et al. 2000 and references therein) that these repeated crossings of the shock result in a power-

law particle distribution with a well-defined index  $p = -2.23$ , which would give a high-energy synchrotron photon index  $\beta$  of  $-1.62$  (or  $-2.12$  for the “cooling” spectrum; see, e.g., Sari, Piran, & Narayan 1998). Although this is consistent with some afterglows, this is certainly not true for many bursts in the prompt phase. In our synchrotron models above, the high-energy photon index  $\beta = -(p + 1)/2$ , where  $p$  is the high-energy index of the emitting particle distribution. The parameter  $\beta$  can vary by a factor of 4 (or more!) throughout a single burst (see, e.g., Preece et al. 2000), reflecting a huge variation (from 1 to 9) in the parameter  $p$  of the underlying particle distribution—this is well beyond the statistical limits placed on  $p$  by shock acceleration simulations. In addition, shock acceleration predicts an *isotropic* distribution of electrons. Our work suggests that in a large fraction of GRBs, the particle acceleration is not isotropic but along the magnetic field lines.

In fact, when the Alfvén (phase) velocity  $\beta_A = B/(4\pi n m_p c^2)^{1/2}$  (in units of the speed of light) is greater than 1, stochastic acceleration becomes more efficient than shock acceleration (Dung & Petrosian 1994). It is well known that in this case the electric field fluctuations  $\delta E \sim \beta_A \delta B$  exceed the magnetic field fluctuations, which means a faster acceleration ( $\propto \delta E^2$ ) than scattering rate ( $\propto \delta B^2$ ). Under these conditions, once the particle crosses the shock front into the turbulent region behind the shock, it will undergo stochastic acceleration much faster than it can be turned around to cross the shock again. This is the situation for GRBs, which have inferred magnetic fields of  $B \sim 10^5$  G and densities of  $n \leq 10^8 \text{ cm}^{-3}$  so that  $\beta_A \gg 1$ . The shape of the spectrum is then determined by the relative values of the diffusion coefficients and the rates of energy and pitch angle changes resulting from the interaction of the injected particles with the plasma turbulence behind the shock. Hence, we emphasize the importance of an investigation of particle acceleration in GRB internal shocks.

Last, we would like to emphasize the important role upcoming (and current) GRB missions will have in laying to rest the questions raised in our investigation. With the launch of *HETE-2* and the upcoming launches of *Swift* and the *Gamma-Ray Large Area Space Telescope (GLAST)*, we will be able to get high-quality broadband (from a few eV to GeV) spectra of the prompt GRB emission; such spectra will allow us to test our models more stringently and constrain all of the emission mechanisms that may play a role in GRBs (for example, we may see a synchrotron self-Compton component in the *GLAST* energy range; Dermer, Chiang, & Mitman 2000). Data from these satellites are sure to shed significant light on the photon spectrum and particle acceleration mechanisms in gamma-ray bursts.

We thank the anonymous referee for a careful report, which led to improvements in this paper. We also thank Felix Ryde for interesting discussions. We acknowledge funding by NASA grant NAG 5-7144.

## REFERENCES

- Band, D., et al. 1993, *ApJ*, 413, 281  
 Borgonovo, L., & Ryde, F. 2001, *ApJ*, 548, 770  
 Brainerd, J. J., Preece, R. D., Briggs, M. S., Pendleton, G. N., & Paciesas, W. S. 1996, in *AIP Conf. Proc.* 384, *Gamma-Ray Bursts*, ed. C. Kouveliotou, M. F. Briggs, & G. J. Fishman (New York: AIP), 148  
 Crider, A., et al. 1997, *ApJ*, 479, L39  
 Dermer, C. D., Chiang, J., & Mitman, K. E. 2000, *ApJ*, 537, 785  
 Dung, R., & Petrosian, V. 1994, *ApJ*, 421, 550  
 Epstein, R. I. 1973, *ApJ*, 183, 593  
 Ford, L. A., et al. 1995, *ApJ*, 439, 307  
 Ghisellini, G., Celotti, A., & Lozzati, D. 2000, *MNRAS*, 313, L1  
 Kargatis, V., et al. 1994, *ApJ*, 422, 260  
 Kirk, J. G., Guthmann, A. W., Gallant, Y. A., & Achterberg, A. 2000, *ApJ*, 542, 235  
 Lithwick, Y., & Sari, R. 2001, *ApJ*, 555, 540  
 Lloyd, N. M., & Petrosian, V. 1999, *ApJ*, 511, 550  
 ———. 2000, *ApJ*, 543, 722 (LP00)  
 Lloyd, N. M., Petrosian, V., & Mallozzi, R. S. 2000, *ApJ*, 534, 227

- Mazets, E., Aptekar, R., L., Butterworth, P. S., Cline, T. L., Fredericks, D. D., Golenetskii, S. V., Il'inskii, V. N., & Pal'shin, V. D. 2002, in *Gamma-Ray Bursts in the Afterglow Era: 2nd Workshop*, in press (astro-ph 0102170)
- Mazets, E., Aptekar, R., L., Butterworth, P. S., Cline, T. L., Fredericks, D. D., Golenetskii, S. V., Il'inskii, V. N., & Pal'shin, V. D. 1996, in *AIP Conf. Proc.* 384, *Gamma-Ray Bursts*, ed. C. Kouveliotou, M. F. Briggs, & G. J. Fishman (New York: AIP), 204
- Medvedev, M. V. 2000, *ApJ*, 540, 704
- Medvedev, M. V. & Loeb, A. 1999, *ApJ*, 526, 697
- Norris, J. P., Share, G. H., Messina, D. C., Dennis, B. R., Desai, U. D., Cline, T. L., Matz, S. M., & Chupp, E. L. 1986, *ApJ*, 301, 213
- Pacholczyk, A. G. 1970, *Radio Astrophysics* (San Francisco: Freeman)
- Piran, T. 1999, *Phys. Rep.*, 314, 575
- Preece, R. D., Briggs, M. S., Mallozzi, R. S., Pendleton, G. N., & Paciesas, 2000, *ApJS*, 126, 19
- Preece, R. D., Briggs, M. S., Mallozzi, R. S., Pendleton, G. N., Paciesas, W. S., & Band, D. L. 1998a, *ApJ*, 506, L23
- Preece, R. D., Briggs, M. S., Pendleton, G. N., Paciesas, W. S., Matteson, J. L., Band, D. L., Skelton, R. T., & Meegan, C. A. 1996, *ApJ*, 473, 310
- Preece, R. D., Pendleton, G. N., Briggs, M. S., Mallozzi, R. S., Paciesas, W. S., Band, D. L., Matteson, J. L., & Meegan, C. A. 1998b, *ApJ*, 496, 849
- Pryadko, J. M. & Petrosian, V. 1998, *ApJ*, 495, 377
- Ryde, F., & Svensson, R. 2000, *ApJ*, 529, L13
- . 2002, *ApJ*, submitted
- Sari, R., Piran, T., & Narayan, R. 1998, *ApJ*, 497, L17
- Strohmayer, T. E., Fenimore, E. E., Murakami, T., & Yoshida, A. 1998, *ApJ*, 500, 873
- Tavani, M. 1996, *ApJ*, 466, 768
- Totani, T. 1999, *MNRAS*, 307, L41